

Impact of Manganese incorporation on the structural and magnetic properties of MOCVD-grown $\text{Ga}_{1-x}\text{Mn}_x\text{N}$

Matthew H. Kane^{1,2}, Ali Asghar¹, Martin Strassburg^{1,4}, Qing Song³, Adam M. Payne¹, Christopher J. Summers², Z. John Zhang³, Nikolaus Dietz⁴ and Ian T. Ferguson¹

¹ Georgia Institute of Technology, School of Electrical and Computer Engineering, Atlanta, GA 30332, U.S.A.

² Georgia Institute of Technology, School of Materials Science and Engineering, Atlanta, GA 30332, U.S.A.

³ Georgia Institute of Technology, School of Chemistry and Biochemistry, Atlanta, GA 30332, U.S.A.

⁴ Georgia State University, Department of Physics and Astronomy, Atlanta, GA 30303, U.S.A.

*ianf@ece.gatech.edu

ABSTRACT

This paper reports the impact of the Mn incorporation on the structural and magnetic properties of $\text{Ga}_{1-x}\text{Mn}_x\text{N}$ on the metal-organic vapor phase deposition (MOCVD). Crystalline quality and phase purity were determined by high-resolution X-ray diffraction and indicated that no macroscopic second phases are formed during growth. Atomic force microscopy revealed a 2-dimensional MOCVD step-flow growth pattern in the Mn-incorporated samples. Various annealing steps were applied to some of the samples to reduce compensating defects and to investigate the effects of post processing on the growth. SQUID measurements showed an apparent ferromagnetic hysteresis behavior. However, none of the requirements for room temperature ferromagnetism in the prevailing mean field DMS theories were found. Therefore, different origins of the ferromagnetic signal are discussed.

INTRODUCTION

Diluted magnetic semiconductors (DMS) are attractive candidates for the next generation of electronic devices which can exploit both the spin and charge of an electron for computational, logic, and storage operations. These materials consist of a traditional III-V, II-VI, or group IV semiconductor into which a small fraction of a magnetic element, such as interior transition metal like Mn, has been introduced. Some DMS materials can exhibit ferromagnetic behavior under certain doping and processing conditions. These ferromagnetic materials could provide a stable source of spin polarized carriers, which combined with the ease of integration into existing semiconductor technology, may enable future spintronic devices in these DMS systems.

Traditional III-V DMS, such as $\text{Ga}_{1-x}\text{Mn}_x\text{As}$, are well-established, though the Curie temperatures of these materials are limited to only around 170K [1]. The ferromagnetic ordering is thought to originate from a long range coupling of the magnetic centers through the free hole carriers [2]. When applying this mean field model to the GaN system, the Curie temperature is predicted to be above room temperature, though this model requires larger substitutional Mn concentrations (~5%) and hole concentrations (3.5×10^{20}) than may be achievable in the $\text{Ga}_{1-x}\text{Mn}_x\text{N}$ system. Other models have been developed based on first principles density functional theory calculations using the local spin density approximation that also predict ferromagnetism in the nitride compounds [3-5]. In these models, the Mn 3d levels are not

strongly hybridized with the GaN (s,p) levels as is seen in $\text{Ga}_{1-x}\text{Mn}_x\text{As}$; nevertheless, ferromagnetism is expected in this system. The double exchange mechanism results in a midgap manganese related impurity band. Ferromagnetism can be stabilized if the Fermi level is within this impurity band because the density of states function is split into a half metallic like structure. It should be noted that the exact mechanism of ferromagnetism in the wide bandgap semiconductors is still a subject of much controversy.

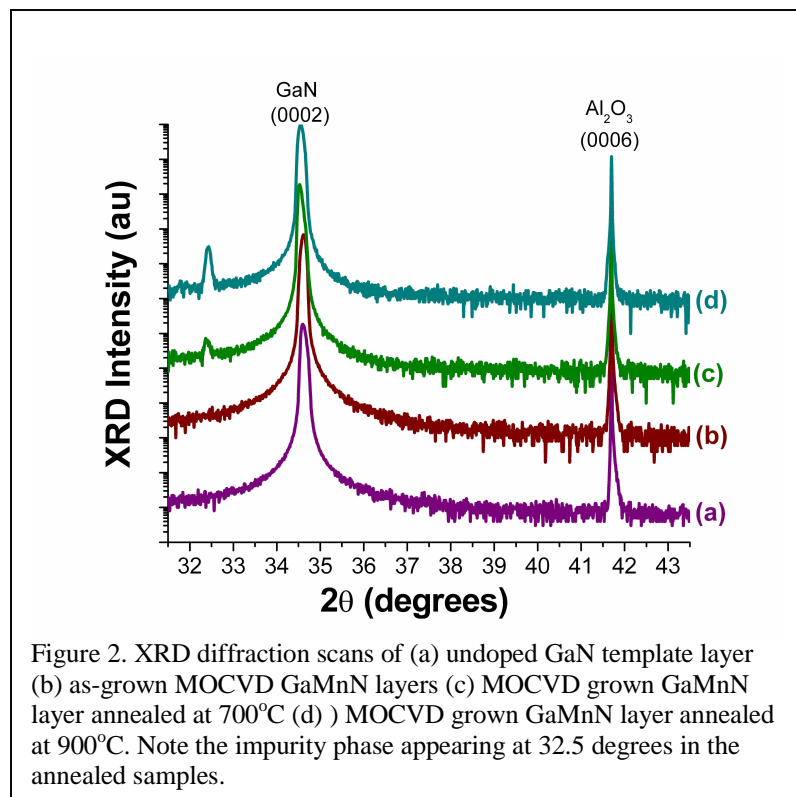
It is imperative to understand both the non-equilibrium growth processes involved as well as the effects of any post-growth processing on these material systems because these compounds are inherently non-equilibrium. For example, $\text{Ga}_{1-x}\text{Mn}_x\text{As}$ is grown almost exclusively by low temperature molecular beam epitaxy [1,6], and during growth and annealing there is always a competition between the dilute $\text{Ga}_{1-x}\text{Mn}_x\text{As}$ phase and the MnAs second phase. Careful low temperature annealing can result in improved magnetic behavior due to the reduction of Mn interstitials [7], but at elevated temperatures can result in second phase segregation [8]. The growth and annealing effects in $\text{Ga}_{1-x}\text{Mn}_x\text{N}$ are less well established. As many of the initial results for $\text{Ga}_{1-x}\text{Mn}_x\text{N}$ were of implanted material [9,10], there would always be some post processing required when using this technique. Excessive annealing was also found to produce second phases in as-grown and implanted material, though the exact phase produced varied from Mn_3N_2 and $\text{Mn}_6\text{N}_{2.58}$ [11] to GaMn intermetallics [12] to Mn_3GaN [13,14] depending on the processing conditions. Ultimately, the optimal growth and processing path for room temperature ferromagnetic GaMnN must be understood.

EXPERIMENTAL

The growth was performed in an Emcore MOCVD D-125 rotating disk reactor with a short jar configuration. The reactor has a specially modified flow flange injection system which has been modified with dual injector blocks to minimize pre-reactions of the gallium and manganese precursors in the transport phase. Mn concentration in the film was varied up to ~2% by controlling the molar flow ratios of the precursors. Initially, two micron thick GaN buffer layer templates were grown using standard GaN techniques on two-inch c-cut sapphire wafers. Ammonia, trimethyl gallium (TMG) and bis-cyclopentadienyl manganese (Cp_2Mn), bis-cyclopentadienyl magnesium (Cp_2Mg) and silane (SiH_4) were used as the nitrogen, gallium, manganese, p-, and n-dopant sources respectively for $\text{Ga}_{1-x}\text{Mn}_x\text{N}$. A 300nm GaN capping layer was deposited on top of some samples in order to provide a non-manganese terminated surface for annealing studies. Some samples were subsequently annealed face-down on GaN templates in a flowing nitrogen ambient at temperatures ranging from 700°C to 900°C. Detailed characterization of these films was performed, including X-ray diffraction (XRD), secondary ion mass spectroscopy (SIMS), atomic force microscopy (AFM), superconducting quantum interference device magnetometry (SQUID), and electrical transport measurements.

RESULTS AND DISCUSSION

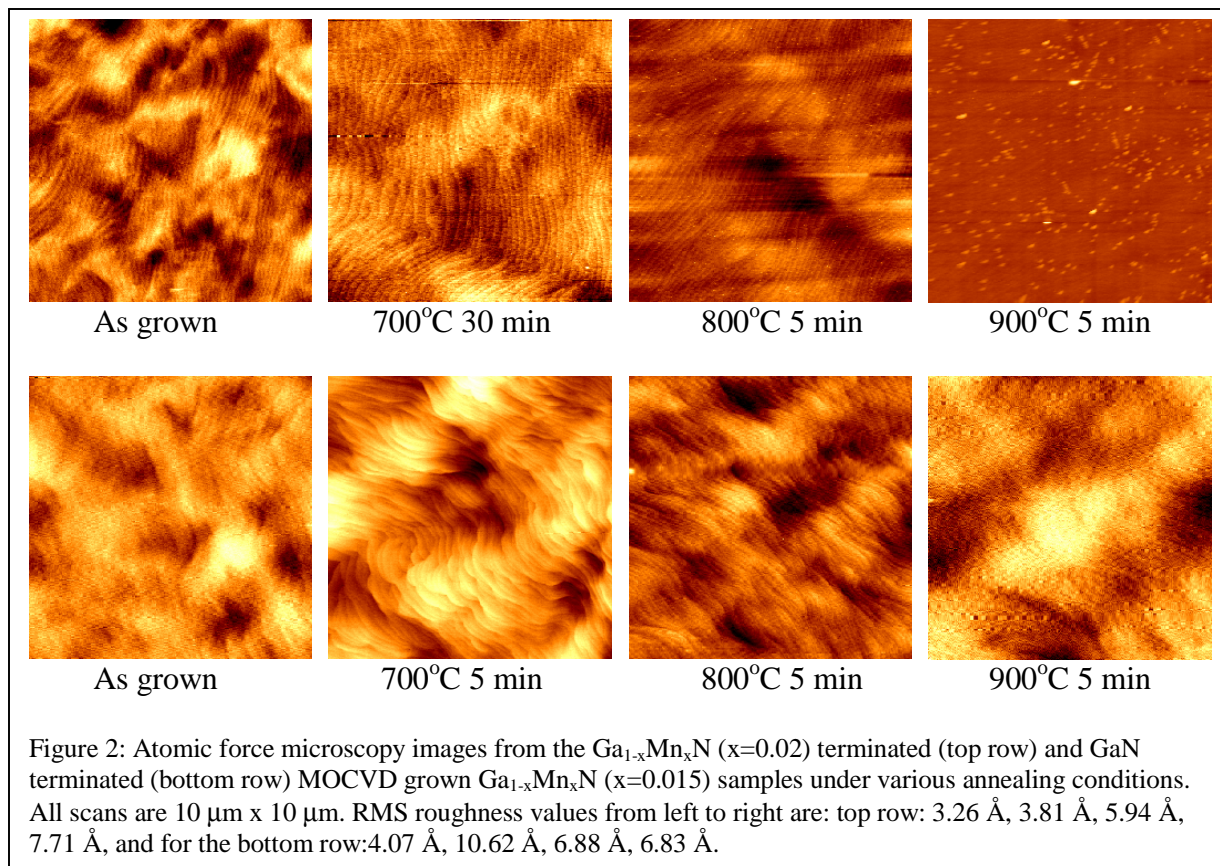
The as-grown films are specular and had an increasing reddish tint with increasing Mn concentration. Varying the temperature outside the optimal growth band resulted in the appearance of hexagonal GaN growth temperature defects which were visible via optical microscopy, or the loss of film integrity. Secondary ion mass spectroscopy verified a uniform incorporation of manganese within the layers. High resolution x-ray diffraction was performed in order to examine the phase purity and crystalline quality of the as-grown films. In the x-ray diffraction scans, no second phases were observed in the as-grown scans, as seen in Figure 1.



phase which has been reported to be present [12]. This second phase is not observed in the samples capped with a thin GaN layer, even at annealing temperatures of 900°C, though further investigations are required to determine the post-annealing phase purity of the capped samples. The $\text{Mn}_6\text{N}_{2.58}$ and Mn_3N_2 phases were not observed via XRD in the annealed MOCVD-grown samples as had been previously reported in implanted samples [13].

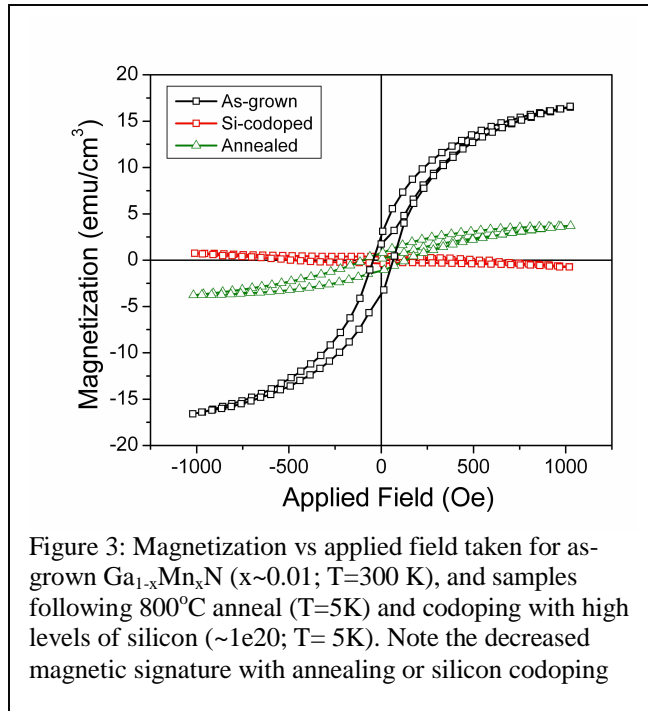
Additional information about the growth mechanism and annealing effects is derived from studies Atomic Force Microscopy (AFM) images of the $\text{Ga}_{1-x}\text{Mn}_x\text{N}$ layers. Figure 2 shows images of the as-grown layers and layers annealed under various temperatures. The overall film quality is smooth with atomic layer surface steps visible. The root mean square (RMS) surface roughnesses are between 4 and 11 Å depending on the film and underlying template layer. Clear step flow growth patterns are seen in the as-grown MOCVD sample scans, which is typical of two-dimensional growth modes seen in GaN MOCVD; this mode does not change with the introduction of manganese into the growth process. Films grown outside the optimal temperature bands exhibit hexagonal GaN temperature defects, and these can be seen in both the AFM as well

The peak position of the $\text{Ga}_{1-x}\text{Mn}_x\text{N}$ peaks did not shift relative to the GaN peaks at the low doping levels, indicating a lattice parameter similar to that of GaN, though this may be influenced by the underlying template layers in some of the films. Rocking curve widths for the (0002) and (10-12) reflections in samples doped at ~1% Mn were 150 and 522 arcsec, compared with 179 and 518 arcsec for the underlying template layer. Upon annealing at temperatures as low as 700°C, other phases do appear in the ω - 2θ scans. These most closely index to the (110) reflections of the $\text{Mn}_{4-x}\text{Ga}_x\text{N}$ phase. This phase has been observed previously [14] though this peak is quite close to a GaMn intermetallic



as via optical microscopy. The RMS roughnesses of the Mn incorporated film is similar to that of the underlying template layer in films doped at $\sim 1\%$ (not shown; $3.8\ \text{\AA}$ vs $3.4\ \text{\AA}$). With low temperature annealing (700°C), there is little change in the morphology of the layer. With annealing at higher temperatures, however, there is a significant difference in the AFM images. The 900°C AFM image of the uncapped sample show clear spots of what is likely second phase precipitate on the surface. Close inspection of the 800°C image shows smaller spots of these second phases which are likely at nucleation sites. On the other hand, the annealed capped samples show no change in surface morphology even at the elevated temperature. This suggests that the primary mechanism for the decay of the thermodynamically unstable $\text{Ga}_{1-x}\text{Mn}_x\text{N}$ compound is through nitrogen desorption and phase rearrangement of the surface at the $\text{Ga}_{1-x}\text{Mn}_x\text{N}$ -to-atmosphere interface possibly due to absence of a reactive nitrogen environment that is present during MBE or MOCVD growth.

SQUID magnetometry was performed to determine the overall magnetic behavior of the MOCVD grown $\text{Ga}_{1-x}\text{Mn}_x\text{N}$ films. Ferromagnetic hysteresis was observed in the as-grown $\text{Ga}_{1-x}\text{Mn}_x\text{N}$ films. No evidence of second phases or superparamagnetic clusters was observed in the magnetic property data. Figure 3 shows representative magnetization behavior of these samples. The curves shown little deviation at $5\ \text{K}$ and $300\ \text{K}$, indicating the hysteresis is due to a phase with a high T_c ($>400\ \text{K}$). The saturation magnetization of the as-grown $\text{Ga}_{1-x}\text{Mn}_x\text{N}$ samples with $x\sim 0.01$ is $11.6\ \text{emu}/\text{cm}^3$, which based on the expected doping levels associated with the precursor molar flows corresponds to a magnetic moment of $2.4\ \mu_B/\text{Mn}$. Upon annealing, this magnetization of the sample drops precipitously, Figure 3. There is still some area remaining in the hysteresis loop observed in this sample, indicating that ferromagnetic phase is not completely lost or there may be a small contribution from ferromagnetic second phases or local



areas of the alloy which were unaffected by the anneal. Reasons for this drop in magnetization could be due to out-diffusion of Mn during the annealing process, conversion of the Mn to a precipitate phase, hydrogen depassivation of Mn or other defects, or increased antiferromagnetic Mn-Mn interactions upon diffusion. A close inspection of the zero field cooled versus field curves temperature dependent magnetization curves indeed shows a small irreversibility which would suggest a minor contribution from nanoscale ferromagnetic phase precipitates. A similar behavior is seen in the MOCVD-grown samples codoped with silicon, where prior to co-doping, a large magnetic moment per atom can be seen, which is nearly destroyed upon doping with silicon at a target doping concentration of $10^{20}/\text{cm}^3$ silicon atoms.

The large decrease in the magnetization with codoping and annealing suggests a common origin to the deterioration of the magnetic properties of $\text{Ga}_{1-x}\text{Mn}_x\text{N}$ with either doping or annealing. The double exchange model of ferromagnetism in the DMS described above can be used to understand this effect. In order to be able to support ferromagnetism, the Fermi level of the system must be in the spin split DOS Mn-impurity band, which is essentially midgap. The Fermi level must lie below the $\text{Mn}^{2+/3+}$ acceptor level so that the T_2 band is only partially filled and can support hopping and double exchange that stabilizes the ferromagnetism. Increasing the Fermi level by introducing donor states above this level results in trapping of donor electrons filling the t_2 band and a conversion from the Mn^{3+} (d^4) to the Mn^{2+} (d^5) configuration, thus eliminating the hopping pathway necessary for ferromagnetic ordering. These donor states may be introduced by either intentional codoping, in the case of silicon codoping, or by the introduction of vacancies and other shallow donor defects during the annealing process. Data reported elsewhere [15] for these same samples shows a close correlation between the optical properties and electron paramagnetic spectrum with the valence state variation and magnetic properties in this system.

SUMMARY AND CONCLUSION

High quality $\text{Ga}_{1-x}\text{Mn}_x\text{N}$ has been grown by metalorganic chemical vapor deposition. Almost no change in the structural properties was observed with Mn incorporation at dilute quantities ($< 2\%$). Upon annealing, the non-equilibrium material decays through a surface decomposition mechanism resulting in secondary phases; terminating the surface with a GaN capping layer prevented this surface decomposition. The as-grown films did exhibit ferromagnetism with relatively high magnetic moments per Mn atom. This strong ferromagnetism could be destroyed through the introduction of shallow compensating donors, either through high temperature annealing processes or through intentional co-doping of the layers with silicon. This is

tentatively attributed to a filling of holes in an Mn impurity band, preventing long range ferromagnetic double exchange coupling of the isolated magnetic centers.

ACKNOWLEDGEMENTS

Work at Georgia Tech has been supported by the Grant #F49620-03-1-0294 from the Air Force Office of Scientific Research (T. Steiner) and the National Science Foundation (ECS 0224266). Support for one author (M.K.) has been provided through a NDSEG fellowship sponsored by the Department of Defense. M.S. gratefully acknowledges the support of the Alexander von Humboldt-Foundation. The authors thank S. Gupta for assistance with some of the AFM measurements.

REFERENCES

- [1] H. Ohno, *Journal of Crystal Growth* **251**, 285-291 (2003).
- [2] T. Dietl, H. Ohno, F. Matsukura, J. Cibert, and D. Ferrand, *Science* **287**, 1019-1022 (2000).
- [3] L. Kronik, M. Jain, and J. R. Chelikowsky, *Physical Review B* **66**, 041203 (2002).
- [4] K. Sato, P. H. Dederichs, H. Katayama-Yoshida, and J. Kudrnovsky, *Physica B* **340-342**, 863–869 (2003).
- [5] K. Sato and H. Katayama-Yoshida, *Semiconductor Science & Technology* **17**, 367-76 (2002).
- [6] H. Ohno, A. Shen, F. Matsukura, A. Oiwa, A. Endo, S. Katsumoto, and Y. Iye, *Applied Physics Letters* **69**, 363-365 (1996).
- [7] T. Wojtowicz, W. L. Lim, X. Liu, Y. Sasaki, U. Bindley, M. Dobrowolska, J. K. Furdyna, K. M. Yu, and W. Walukiewicz, *Journal of Superconductivity* **16**, 41-44 (2003).
- [8] J. D. Boeck, R. Oesterholt, H. Bender, A. V. Esch, C. Bruynseraede, C. V. Hoof, and G. Borghs, *Journal of Magnetism and Magnetic Materials* **156**, 148-150 (1996).
- [9] Y. Shon, Y. H. Kwon, S. U. Yuldashev, J. H. Leem, C. S. Park, D. J. Fu, H. J. Kim, T. W. Kang, and X. J. Fan, *Applied Physics Letters* **81**, 1845-1847 (2002).
- [10] N. Theodoropoulou, A. F. Hebard, M. E. Overberg, C. R. Abernathy, S. J. Pearton, S. N. G. Chu, and R. G. Wilson, *Applied Physics Letters* **78**, 3475-3477 (2001).
- [11] J. M. Baik, H. W. Jang, J. K. Kim, and J.-L. Lee, *Applied Physics Letters* **82**, 583-585 (2003).
- [12] G. T. Thaler, R. M. Frazier, J. Stapleton, C. R. Abernathy, S. J. Pearton, J. Kelly, R. Rairigh, A. F. Hebard, and J. M. Zavada, *Electrochemical and Solid-State Letters* **7**, G34-G36 (2004).
- [13] M. H. Kane, A. Asghar, A. M. Payne, C. R. Vestal, Z. J. Zhang, M. Strassburg, J. Senawirante, N. Dietz, C. J. Summers, and I. T. Ferguson, *Physica Status Solidi C*, Submitted (2004).
- [14] S. Kuroda, E. Bellet-Amalric, X. Biquard, J. Cibert, R. Giraud, S. Marcet, and H. Mariette, *Physica Status Solidi B* **240**, 443-446 (2003).
- [15] M. Strassburg, J. Senawirante, C. Hums, N. Dietz, M. H. Kane, A. Asghar, A. M. Payne, I. T. Ferguson, C. J. Summers, U. Haboek, A. Hoffman, D. Azamat, and W. Gelhoff, *MRS Proceedings*, submitted (2004).